Journal of Alloys and Compounds 506 (2010) 395–399

Contents lists available at ScienceDirect

Journal of Alloys and Compounds

journal homepage: www.elsevier.com/locate/jallcom

Size effect on the magnetic property of $CoAl_2O_4$ nanopowders prepared by reverse micelle processing

J. Chandradass[a], M. Balasubramanian[b], Ki Hyeon Kim[a,*]

[a] Department of Physics, Yeungnam University, Gyeongsan, Gyeongsangbuk-do-712-749, South Korea
[b] Department of Metallurgical and Materials Engineering, Indian Institute of Technology-Madras, Chennai 600036, India

ARTICLE INFO

Article history:
Received 7 May 2010
Received in revised form 2 July 2010
Accepted 6 July 2010
Available online 14 July 2010

Keywords:
Ceramics
Chemical synthesis
Characterization
Nanomaterials
Magnetic property

ABSTRACT

Cobalt aluminate ($CoAl_2O_4$) nanopowders were synthesized by reverse microemulsion process using cyclohexane, a nonionic surfactant, and aqueous solutions of cobalt (II) nitrate hexahydrate and aluminum nitrate nonahydrate. The influence of water to surfactant molar ratio on the size of powders has been studied. The X-ray diffraction analysis shows that the powders calcined at 1000 °C have single phase cubic spinel structure. The average size of the particles increases with increasing water to surfactant molar ratio. The mean diameter of the particles varies between 42 and 57 nm. The Fourier transform infrared spectra also confirm the formation of $CoAl_2O_4$. Magnetization study reveals that the $CoAl_2O_4$ sample exhibits superparamagnetic behavior.

1. Introduction

The synthesis of nano-crystalline spinel has been investigated intensively due to the unique potential applications of nano-crystalline spinels in high density magnetic recording and microwave devices, magnetic fluids, and also as an absorbent material to remove sulfide gases from hot-coal gas [1,2]. Spinel-type pigments are commonly used for decorating porcelain and other ceramic products. The spinels are complex oxides and represented by the general formula of $A^{2+}B^{3+}O_4$. If the bivalent metal is cobalt with a small amount of magnesium, and the trivalent metal is aluminum, then the resulting pigments form blue to sky-blue color range [3]. The common methods reported for the synthesis of cobalt aluminate are sol–gel [4], EDTA chelating precursor [5], combustion [6,7], polymerized complex [8], glycine chelated precursor [9], hydrothermal [10], molten salt [11], polymer aerosol pyrolysis [12], and reverse micelle processes [13,14]. Recently, Yu et al. [15] have reported the synthesis of nanosized $CoAl_2O_4$ spinel powders by using the sol–gel and sol–gel hydrothermal methods. The sol–gel precursor after calcination at 1000 °C for 2 h showed the formation of large and agglomerated $CoAl_2O_4$ spinel powders of particle size, 100–200 nm. Whereas nanosized $CoAl_2O_4$ powders (50–60 nm) were obtained at 250 °C for 24 h by using sol–gel hydrothermal processing. Gama et al. [16] have reported that the Pechini method is an appropriate method for the synthesis of $CoAl_2O_4$, $NiAl_2O_4$ and $ZnAl_2O_4$ nanocrystals. Mindru et al. [17] have reported the synthesis of cobalt–aluminate spinel by the two variants of complexation method: tartarate and gluconate routes. It was found that the presence of tetrahedral coordinated Co^{2+} ion is responsible for the blue bright color. Although, the nanosized spinels of MAl_2O_4 (M = Co, Ni, Cu) were prepared by an emulsion templated hydrolysis of alkoxides, some improvement or optimization of parameter is still required to control the particle size. Moreover, to the best of our knowledge, none of these works have been devoted to the magnetic properties of $CoAl_2O_4$ nanopowders prepared by the reverse micelle process. The aim of the present work is to prepare $CoAl_2O_4$ nanopowders and study their structural and magnetic properties. A tertiary reverse microemulsion system was used to synthesize these nanocrystals. The influence of water to surfactant ratio on the particle size has been studied, since it plays a vital role in controlling the droplet size and hence the size of the crystal. Also, readily available, inexpensive and easy handling precursors have been used in the present study and that eliminates the extra handling requirements associated with the moisture sensitive precursors.

2. Experimental procedures

Fig. 1 shows the flowchart for the preparation of $CoAl_2O_4$ nanopowders by reverse micelle process. Cobalt (II) nitrate hexahydrate ($Co(NO_3)_2{\cdot}6H_2O$), aluminum nitrate nonahydrate ($Al(NO_3)_3{\cdot}9H_2O$) were used as the precursors of cobalt oxide and alumina, respectively. An aqueous solution of the precursors was prepared by dissolving cobalt (II) nitrate hexahydrate (0.1 M) and aluminum nitrate nonahydrate (0.2 M) in distilled water to a molar ratio of 1:2. Cyclohexane (Sigma Aldrich) was used as the solvent. Reverse microemulsion was prepared by mixing 40 mL of

* Corresponding author. Tel.: +82 53 810 2334; fax: +82 53 810 4616.
E-mail address: kee1@ynu.ac.kr (K.H. Kim).

0925-8388/$ – see front matter © 2010 Elsevier B.V. All rights reserved.
doi:10.1016/j.jallcom.2010.07.014

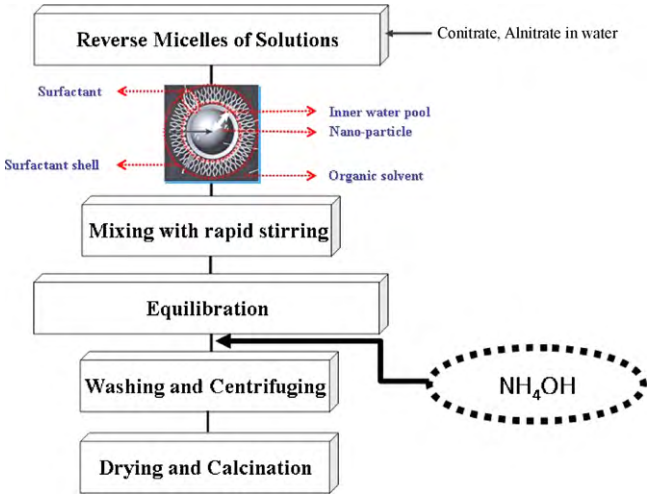

Fig. 1. Flowchart for the preparation of $CoAl_2O_4$ powders by reverse micelle processing.

nonionic surfactant (poly(oxyethylene) nonylphenyl ether, Igepal CO-520, Aldrich, USA), 100 ml of cyclohexane and 6–13.2 ml of mixed aqueous solution (Co:Al = 1:2). The microemulsion was stirred vigorously, and after 5 min of equilibration, 3–6 ml of NH_4OH (28%) (Dae Jung chemicals, Korea) was injected into the microemulsion. The microemulsion was then centrifuged to extract the particles, and the particles were subsequently washed using ethanol to remove any residual surfactant. The thermal characteristics of the powders were determined by thermogravimetry (TG) and differential thermal analysis (DTA) techniques (SCINCO, STA 1500). The phase identification of calcined powders was carried out by X-ray diffractometer (Philips X'pert MPD 3040). The particle size of the calcined powders was analyzed using Transmission electron microscope (TEM) operating at an accelerating voltage of 200 kV (JEOL, JEM 2100F). The average size of the particles was estimated from the TEM micrographs using standard software (IMAGE J). The Fourier transform infrared spectra (FTIR) of the samples were obtained using Nicolet Impact 410 DSP spectrophotometer by the KBr pellet method. The magnetic measurements of the samples were performed on a PPMS-physical property measurement system (Quantum Design, Inc.).

3. Results and discussion

The thermo-chemical behavior of dried $CoAl_2O_4$ powder is shown in Fig. 2. There are three distinct regions in the TG curve. The initial weight loss in the region RT–200 °C corresponds to the volatilization of organic substances, or moisture existing in the precipitated powders. In the temperature region between 200 and 400 °C, the weight loss is caused by the decomposition of organic compounds [14]. The third weight loss occurring over a broad range of temperature is attributed to the pyrolytic elimination of residual hydroxyl groups, etc. [14]. After 1000 °C, the weight of the sample is constant, which indicates the completion of decomposition and the formation of $CoAl_2O_4$ crystals. The thermal decomposition behavior is associated with the endothermic and exothermic effects. The first weight loss due to the removal of adsorbed water is indicated by a small endothermic peak around 50 °C in the DTA curve. An exothermic peak at 260 °C in the DTA curve is due to the decomposition of residual surfactant.

The XRD patterns of the powders calcined at 1000 °C are shown in Fig. 3. Extremely broad peaks are observed and those indicate the presence of very fine particles. The observed diffraction peaks correspond to the standard patterns of $CoAl_2O_4$ spinel (ICSD 01-082-2251). No other crystalline phases are found in the calcined samples. The broadening of XRD peaks increases as the water to surfactant ratio is decreased for the preparation of powder. The crystallite size of powders obtained using different water to surfactant ratio is given in Table 1. The average crystallite size of the powders increases as the water to surfactant ratio (R) is increased from 4 to 8 during the preparation of powder.

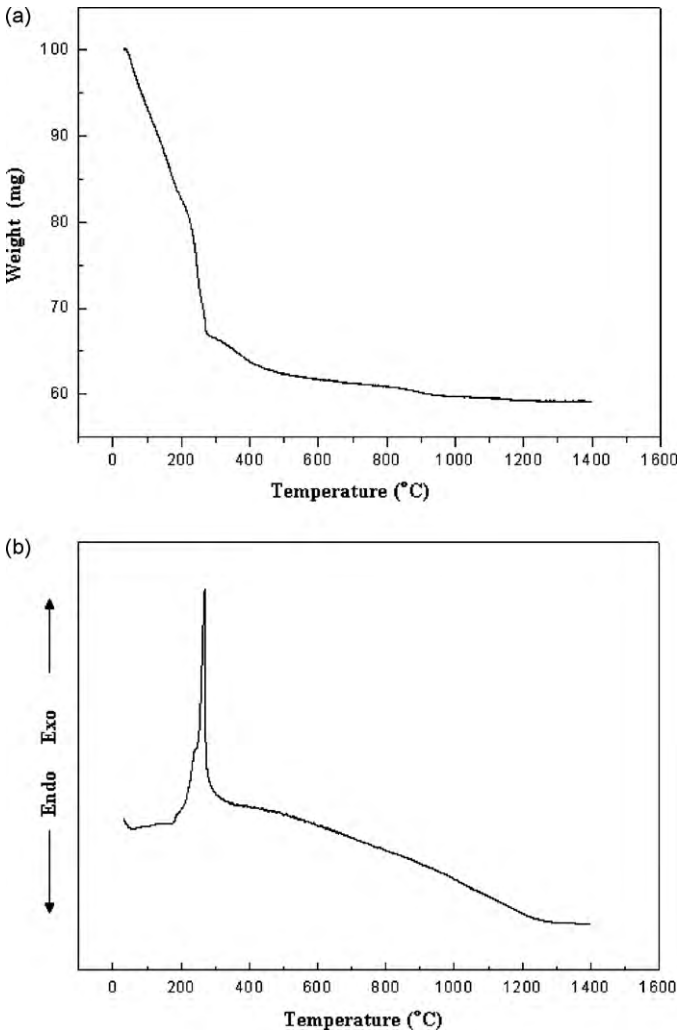

Fig. 2. DTA and TGA of as-synthesized powders.

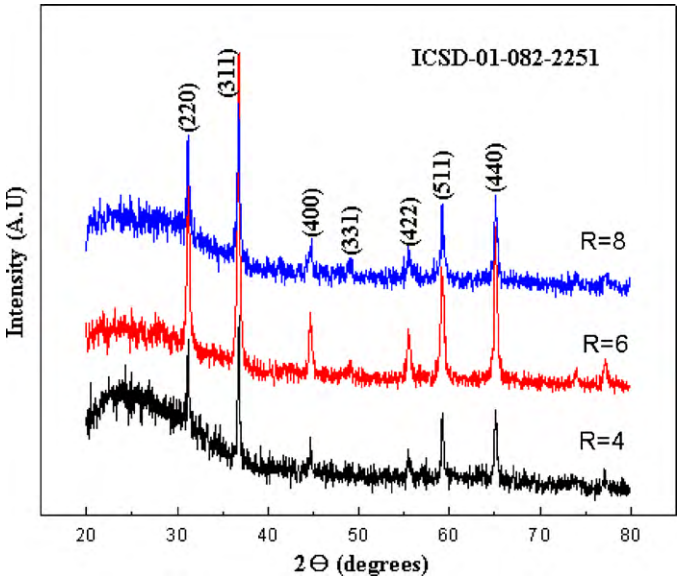

Fig. 3. X-ray diffraction patterns of powders calcined at 1000 °C.

Table 1
Crystallite size, particle size and saturation magnetization of $CoAl_2O_4$.

Water to surfactant molar ratio	Crystallite size (XRD) (nm)	Particle size (TEM) (nm)	Saturation magnetization (M_s) (emu/g)
4	26	35	0.028
6	32	40	0.086
8	35	57	0.23

Fig. 4 shows the TEM micrographs of powders synthesized using various R values and calcined at 1000 °C. It can be seen that the nanoparticles are nearly spherical with narrow particle size distribution. The average particle size of calcined powder increases from 42 to 57 nm as the R value increases from 4 to 8. The nucleation and growth are controlled by interaction between micelles, phase behavior and solubility, average occupancy of the reacting species in the aqueous medium, dynamic behavior of the reverse micellar solution and so on [18]. Munshi et al. [19] have reported that the size of the particles formed in the reverse micelles is larger than the hydrodynamic size of the reverse micellar droplets in which the particles are formed. This is known to be due to the partial cluster formation of the micellar droplets, which is affected by temperature and micellar size. Moreover, by increasing the water to surfactant ratio, one would expect that the nanoparticles size should increase. Therefore, by changing these parameters, the size of nanoparticles has been controlled [20]. The average particle size obtained from TEM technique is larger than that observed from X-ray line broadening technique. It may be due to the formation of agglomerates.

Fig. 5 shows the FTIR spectra of the dried powder synthesized using the R value of 4 and the corresponding calcined powder. The band at 3470 cm^{-1} in the dried powder is attributed to the stretching vibrations of the hydrogen-bonded OH groups. The absorption band at 2964 cm^{-1} is related to C–H stretching vibration from the organic compounds. The absorption band in the region 2100 cm^{-1} indicates the presence of hydrogen-bonded OH [21]. The characteristics stretching bands between 1590 and 1720 cm^{-1} are due to –COOH stretching vibrations [22,23]. The ν_3 mode of the CO_3^{2-} anion appeared around 1384 cm^{-1} [24]. However, the bands due to

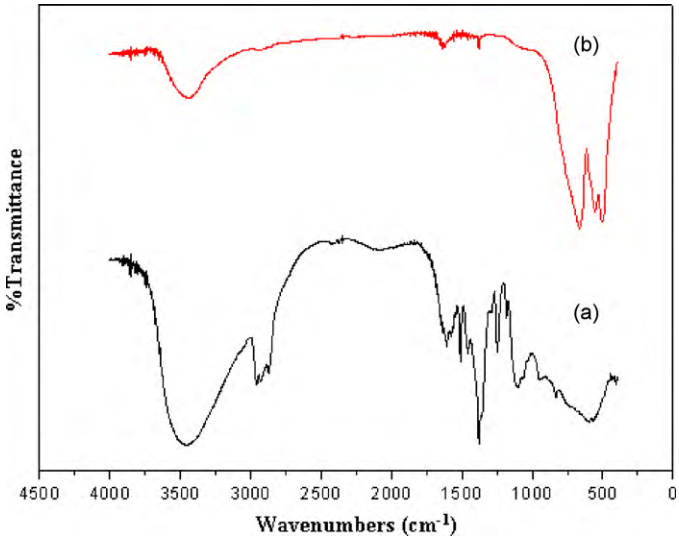

Fig. 5. FTIR analysis of $CoAl_2O_4$ powder prepared using $R = 4$: (a) dried; (b) calcined at 1000 °C.

the stretch vibrations of NO_3^- are evident at 1245 cm^{-1} [25,26]. The absorption band at 1097 cm^{-1} is probably due to CH–OH stretching vibration [22]. The visible bands over the range of 1000–400 cm^{-1} correspond to metal–oxygen bonds (Co–O and Al–O stretching) vibrations for the spinel structure compound. The presence of –OH group in the calcined samples is possibly due to moisture absorption. New bands at 662, 550 and 499 cm^{-1} of the calcined powders indicate the formation of metal oxide, and that is already confirmed by XRD (Fig. 2).

Fig. 6 shows magnetization (M) versus applied magnetic field (H) at room temperature for the samples made with powders synthesized using different water to surfactant ratio. The absence of hysteresis loop, remanence and coercivity at 300 K on all samples are indicative of the presence of superparamagnetic and single domain crystals [27]. The superparamagnetic behavior at room temperature means that the thermal energy can overcome the

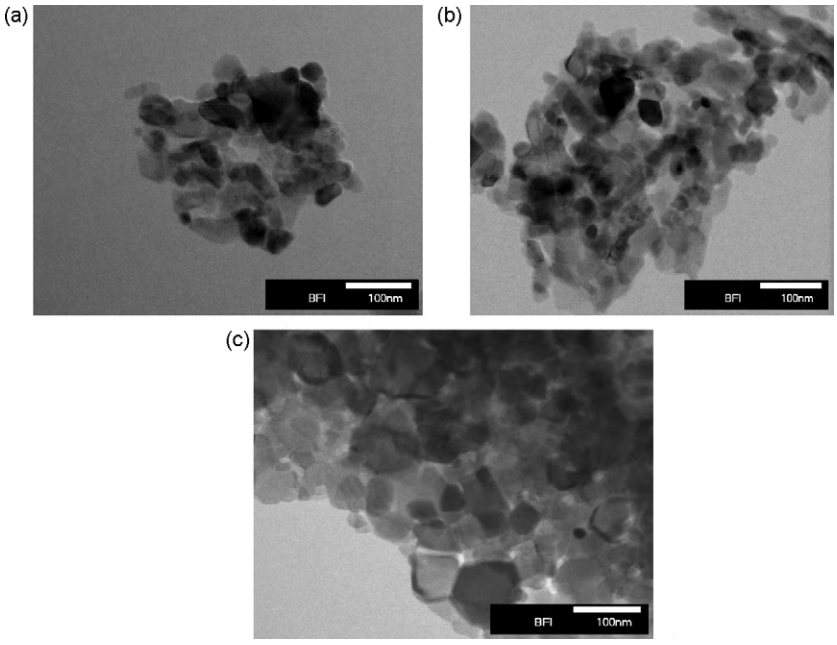

Fig. 4. TEM micrographs of powders calcined at 1000 °C: (a) $R = 4$; (b) $R = 6$; (c) $R = 8$.

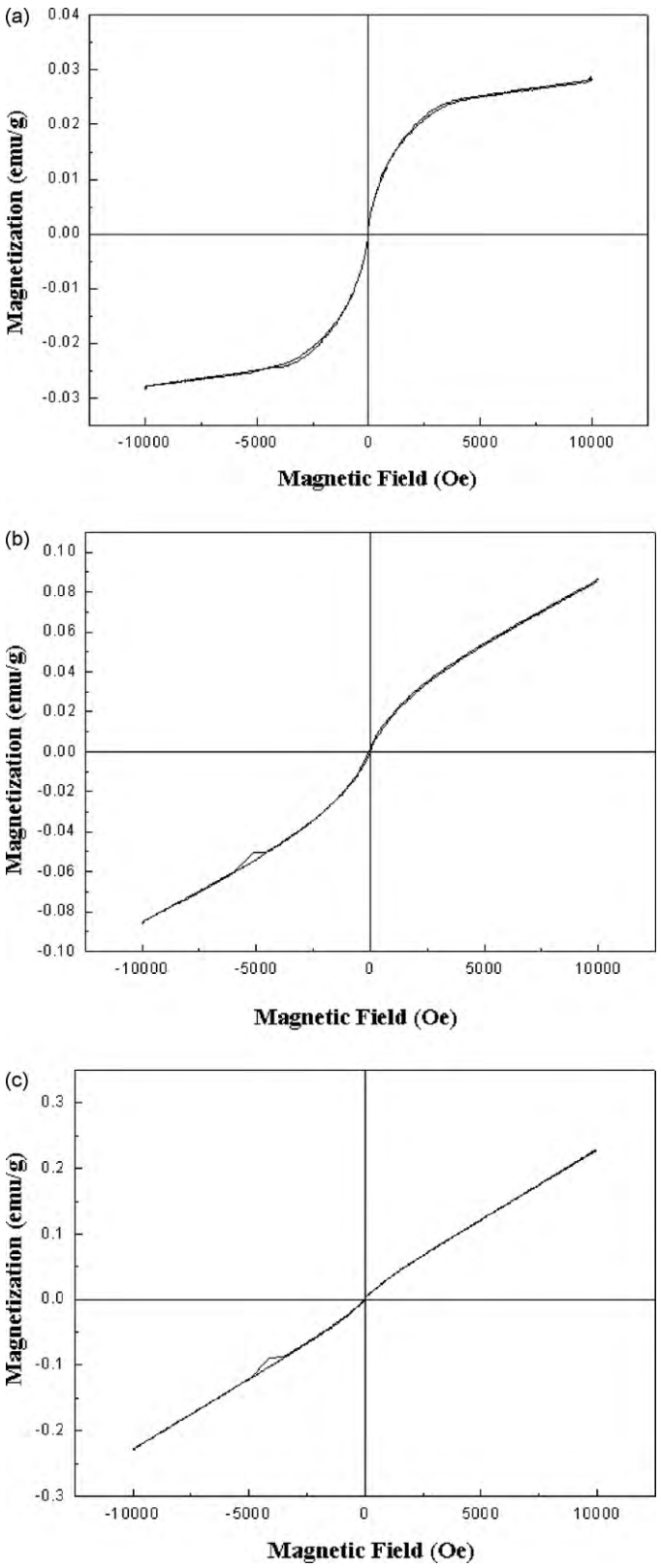

Fig. 6. *M–H* curves for $CoAl_2O_4$ samples at room temperature (a) $R = 4$; (b) $R = 6$; (c) $R = 8$.

anisotropy energy barrier of a single particle, and the net magnetization of the particles in the absence of an external field is zero [28]. The deduced value of saturation magnetization is given in Table 1. The M_S values of samples are 0.028, 0.086 and 0.23 emu/g, when the powders are synthesized with R values of 4, 6 and 8, respectively. The saturation magnetization increases with increase in particle size. Surface effect can lead to reduced magnetization in small ferrite particles. This reduction is associated with different mechanisms, such as the existence of a magnetically dead layer on the particles surface, the existence of canted spin or the existence of a spin glass like behavior of the surface spins [29]. Another surface-driven effect is the enhancement of the magnetic anisotropy (K_{eff}) with decreasing particle size [30,31]. In addition to the surface effect, the order–disorder characteristic of the samples has also a strong influence on the decrease of saturation magnetization [32]. For the samples prepared using powders synthesized with the water to surfactant ratio of 8, the superparamagnetic behavior is characterized by higher saturation magnetization (M_S). The relatively higher saturation value may be due to the fact that the anisotropic features of these nanocrystals have enhanced dipole–dipole interaction, favoring a head-to-tail orientation [33].

4. Conclusions

Single phase cobalt aluminate ($CoAl_2O_4$) nanopowders can be prepared using the precipitation of hydroxides and their oxidation from the reverse microemulsions of the aqueous solution. The size of the nanoparticles can be controlled by the concentration of the reactants in the aqueous solutions of the microemulsions. The particle size increases with the increasing water to surfactant ratio. The specific magnetization, which depends mainly on the particle size, ranged from 0.028 emu g^{-1} for the particles of approximately 35 nm in size, to 0.23 emu g^{-1} for the particles of approximately 57 nm in size.

References

[1] S. Bid, S.K. Pradan, Mater. Chem. Phys. 82 (2003) 27–37.
[2] R.E. Ayala, D.W. Marsh, Ind. Chem. Res. 30 (1991) 55–60.
[3] N.I. Radishevskaya, N.G. Kasatskii, A.Yu Chapskaya, O.K. Lepakova, V.D. Kitler, Yu.S. Naiborodenko, V.V. Vereshchagin, Glass Ceram. 63 (2006) 52–54.
[4] M. Zayat, D. Levy, J. Sol–Gel Sci. Technol. 25 (2002) 201–206.
[5] C. Wang, X. Bai, S. Liu, L. Liu, J. Mater. Sci. 39 (2004) 6191–6201.
[6] W. Li, J. Li, J. Guo, J. Eur. Ceram. Soc. 23 (2003) 2289–2295.
[7] T. Mimani, J. Alloys Compd. 315 (2001) 123–128.
[8] W.-S. Choa, M. Kakihanab, J. Alloys Compd. 287 (1999) 87–90.
[9] C. Wang, S. Liu, L. Liu, X. Bai, Mater. Chem. Phys. 96 (2006) 361–370.
[10] Z.-Z. Chen, E.-W. Shi, W.-J. Li, Y.-Q. Zheng, J.-Y. Zhuang, B. Xiao, L.-A. Tang, Mater. Sci. Eng. B107 (2004) 217–223.
[11] N. Ouahdi, S. Guillemet, B. Durand, R. El Ouatib, L. Er Rakhob, R. Moussab, A. Samdi, J. Eur. Ceram. Soc. 28 (2008) 1987–1994.
[12] H. Guorong, D. Xinrong, C. Yanbing, P. Zhongdong, Rare Met. 26 (2007) 236–241.
[13] F. Meyer, A. Dierstein, Ch. Beck, W. Hlirtl, R. Hempelmanu, S. Mathur, M. Veith, Nanostruct. Mater. 12 (1999) 71–74.
[14] F. Meyer, R. Hempelmann, S. Mathur, M. Veith, J. Mater. Chem. 9 (1999) 1755–1763.
[15] F. Yu, J. Yang, J. Ma, J. Du, Y. Zhou, J. Alloys Compd. 468 (2009) 443–446.
[16] L. Gama, M.A. Ribeiro, B.S. Barros, R.H.A. Kiminami, I.T. Weber, A.C.F.M. Costa, J. Alloys Compd. 483 (2009) 453–455.
[17] I. Mindru, G. Marinescu, D. Gingasu, L. Patrona, C. Ghicab, M. Giurgincac, Mater. Chem. Phys. 122 (2010) 491–497.
[18] C. Petit, P. Lixon, M.P. Pileni, J. Phys. Chem. 97 (1993) 12974–12983.
[19] N. Munshi, T.K. De, A.N. Maitra, J. Colloid Interface Sci. 190 (1997) 387–391.
[20] M. Ghiaci, H. Aghaei, A. Abbaspur, Mater. Res. Bull. 43 (2008) 1255–1262.
[21] V. Saraswathi, G.V.N. Rao, G.V. Rama Rao, J. Mater. Sci. 22 (1987) 2529–2534.
[22] K. Nakamoto, Infrared and Raman Spectra of Inorganic and Coordination Compounds, John Wiley & Sons, New York, 1986.
[23] B. Schrader (Ed.), Infrared Raman Spectroscopy: Methods and Applications, VCH, Weinheim, 1995.
[24] R.A. Nyquist, R.O. Kagel, Infrared Spectra of Inorganic Compounds (3800–45 cm^{-1}), Academic Press, New York, 1971.
[25] J. Livage, M. Henry, C. Sanchez, Prog. Solid State Chem. 18 (1988) 259–341.
[26] C.J. Brinker, G.W. Scherrer, Sol–Gel Science: The Physics and Chemistry of Sol–Gel Processing, Academic Press, New York, 1990.
[27] T. Upadhyay, R.V. Upadhyay, R.V. Mehta, Phys. Rev. B 55 (1997) 5585–5588.
[28] S. Sun, H. Zheng, D.B. Robinson, S. Raoux, P.M. Rice, S.X. Wang, G. Li, J. Am. Chem. Soc. 126 (2004) 273–279.
[29] R.H. Kodama, J. Magn. Magn. Mater. 200 (1999) 359–372.

[30] M. Respaud, J.M. Broto, H. Rakoto, A.R. Fert, L. Thomas, B. Barbara, M. Verelst, E. Snoeck, P. Lecante, A. Mosset, J. Osuna, T. Ould Ely, C. Amiens, B. Chaudret, Phys. Rev. Lett. 57 (1998) 2925–2935.
[31] F. Bodker, S. Morup, S. Linderoth, Phys. Rev. Lett. 72 (1994) 282–285.
[32] Sanjeev Kumar, Vaishali Singh, Saroj Aggarwal, Uttam Kumar Mandal, Ravinder Kumar Kotnala, J. Phys. Chem. C, doi:10.1021/jp911586d.
[33] D. Yu, X. Sun, J. Zou, Z. Wang, F. Wang, K. Tang, J. Phys. Chem. B 110 (2006) 21667–21671.